International Journal of Concrete Structures and Materials

RESEARCH

Open Access

Tensile Performance, Lap-Splice Length and Behavior of Concretes Confined by Prefabricated C-FRCM System

Donguk Choi[1], Sorrasak Vachirapanyakun[2*], Munckhtuvshin Ochirbud[1], Undram Naidangjav[1], Sangsu Ha[3] and Youngho Kim[4]

Abstract

Results of an experimental study aimed to evaluate tensile performance, lap-splice length of carbon fabric-reinforced cementitious matrix system (C-FRCM), and performance of concretes confined by C-FRCM are presented. Green high-strength mortar was used in this study which actively utilized recycled fine aggregate and fine waste glass powder to partially substitute cementitious binder. Test plans were developed in due consideration of prefabricated C-FRCM for strengthening concrete columns: 14 tensile tests, 12 lap-splice tests, and 6 uniaxial compression tests of plain concrete specimens confined by C-FRCM were performed. Test variable for the tensile test was number of fabric layers (one or two layers). Nominal strength of the C-FRCM with two fabric layers was 11.0 MPa while it was 7.4 MPa with one fabric layer in tension. Full strength of the carbon fabric was developed in all tensile tests while the C-FRCM with two fabric layers (with axial fiber amount = 0.59% by vol.) showed pseudo-ductile behavior. From the lap-splice tests in direct tension, an increased lap-splice length was required for the double fabrics over that for the single fabrics. The required splice length was about 170 mm for the single fabrics and it was about 310 mm for the double fabrics. Plain concrete cylinders and prismatic specimens were laterally confined by C-FRCM and subjected to uniaxial compression. All test results showed strain-softening behavior. Compressive strength increased by 10–41% while ductility also increased by 6–45% indicating applicability of the prefabricated type C-FRCM in the future.

Keywords: carbon fabric, tensile performance, lap splice, confinement, prefabricated FRCM, green high-strength mortar

1 Introduction

The fabric-reinforced cementitious matrix (FRCM) system evolved from ferrocement where the metallic reinforcement is replaced by fabrics of dry fibers (ACI 549.4R-13): i.e. single or multiple layers of 2D (or 3D) fabrics are impregnated by inorganic matrix such as cementitious mortar, lime mortar, or mortar comprising cement and polymers. The FRCM system is called textile-reinforced concrete or mortar (TRC or TRM) in Europe. Low-to-normal strength inorganic matrices with 10–45 MPa compressive strength typically have been utilized when the FRCM systems are used toward external strengthening of the masonry elements such as masonry walls (Caggegi et al., 2017; Carozzi et al., 2017; Leone et al., 2017; Koutas et al. 2019). The FRCM systems are also applied to externally strengthen reinforced concrete (RC) members such as RC beams, slabs, columns, walls, and beam–column joints (Donnini et al., 2019b; Hadad et al., 2018; Larbi et al., 2013; Tello et al., 2021). The FRCM system has advantages over the external FRP strengthening, such as its applicability on wet surfaces, good performance under elevated temperatures

*Correspondence: sornthelight@gmail.com
[2] Department of Civil and Environmental System Engineering, Konkuk University, Seoul 05029, Republic of Korea
Full list of author information is available at the end of the article
Journal information: ISSN 1976-0485 / eISSN 2234-1315

in addition to so called "breathability" of the inorganic matrix as compared to the much denser polymer impregnation of fibers of the FRP. One to several layers of fabrics made of various fibers such as carbon fiber, glass fiber, aramid fiber, basalt fiber, and polyparaphenylene benzobisoxazole fiber (PBO) have been used. Some researchers tried to use the strain-hardening type cementitious matrix (Al-Gemeel & Zhuge, 2018; Gong et al., 2020). Others tried multiple layers of the fabric embedded in the pressurized dense mortar (Peled et al., 2009).

In this study, carbon fiber-reinforced cementitious matrix system (C-FRCM) is utilized: i.e. carbon fiber (CF) was used in a form of 2D fabric along with a green high-strength mortar utilizing recycled materials such as finely ground waste glass powder and recycled fine aggregate. The experimental programs included tests for the basic mechanical characterization (tensile test and lap-splice test) and tests for the application of the C-FRCM for the purpose of concrete column strengthening. The C-FRCM considered in this study includes potential application in a form of the prefabricated FRCM (You et al., 2020).

It is well known that two different approaches exist when evaluating the tensile performance of a FRCM system. In one approach, a clamping grip is used. The ends of the thin and prismatic specimens are subjected to out-of-plane compressive stress applied by a hydraulic means (such as the hydraulic grip of UTM) during test. Resulting tensile behavior of the FRCM system is typically tri-linear as shown in Fig. 1a: (1) linear behavior to the first cracking in the uncracked phase; (2) stable behavior with slowly increasing resistance accompanied by intermittent load drop and recovery due to mortar cracking during the cracking phase; and (3) linear behavior up to the ultimate in the cracked phase. The stiffness of the FRCM system is usually the same as that of the sum of all axial fibers in the cracked phase as resistance of the mortar is lost due to crack(s). This approach was adopted by Caggegi et al. (2017), Carozzi et al. (2017), Leone et al. (2017), Santis et al. (2017), and Antino and Papanicolaou (2018). In the other approach, thin rectangular tensile test specimens are also used while a clevis grip is utilized. The tensile behavior of the FRCM system determined by using the clevis grip is typically bilinear as shown in Fig. 1b: (1) linear behavior to the cracking stage (or to transition point where two idealized lines meet in Fig. 1b) followed by (2) linear behavior to the ultimate stage. As this test method allows slip of the fibers through the mortar, the stiffness of the FRCM system is less than that determined by the clamping grip. This approach has been used by Donnini et al. (2019a), Mazzuca et al. (2019), and Hadad et al. (2020). The first approach in general follows recommendation of Rilem 232-TDT (2016) and can be used to obtain a complete mechanical characterization including tensile failure of each constituent material. The second approach is usually conducted according to Annex A of AC434 (2013) and can be used to determine design parameters considering boundary conditions in the field (Arboleda et al., 2016). It is noted that other researchers also used the dumbbell coupons or the ring specimens when the strain-hardening cement-based composites were used (Al-Gemeel & Zhuge, 2018; Gong et al., 2020).

Several researchers investigated the bond behavior of the various FRCM systems using single- or double-lap shear test setup (Bellini et al., 2019; Raoof et al., 2016;

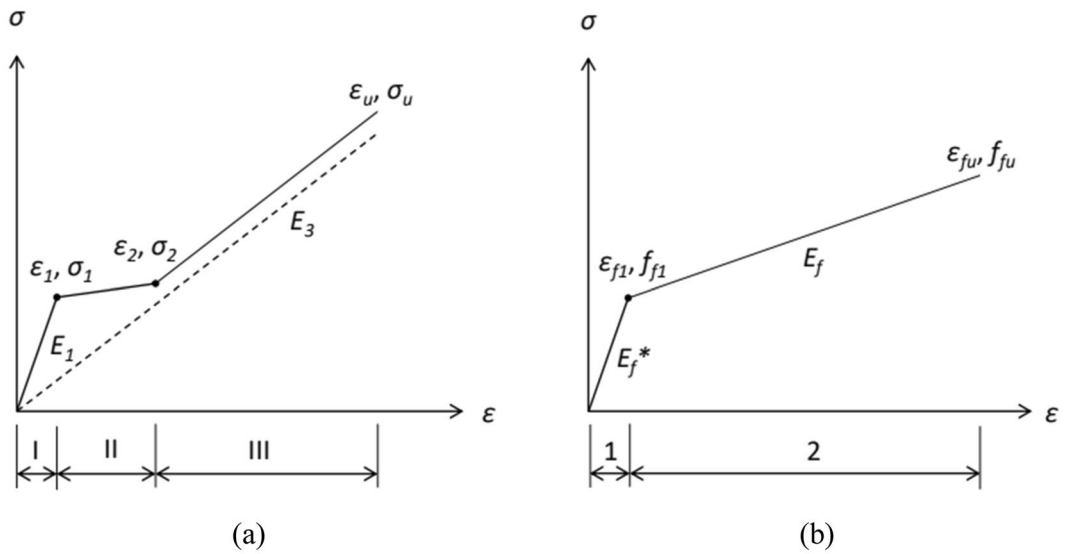

Fig. 1 Idealized stress–strain relationships of FRCM system in tension: **a** tri-linear relationship; **b** bi-linear relationship.

Younis & Ebead, 2018). Raoof et al. (2016) used carbon fiber textile and mortars comprising cement and polymers. The effective bond length was in the range of 200–300 mm for the examined number of layers (1–4 layers). For the one and two TRM layers, the failure was due to slippage of the textile fibers through the mortar. On the other hand, the failure was attributed to debonding at the mortar/concrete interface for the three and four layers. Coating the textile with epoxy adhesive had a two-fold effect: (1) change in the failure mode from slippage through the mortar to TRM debonding at textile/mortar interface; and (2) bond strength increase.

Younis and Ebead (2018) performed double shear tests using three different fabrics made of PBO, carbon fiber, and glass fiber and low-to-normal strength cement mortars (20–40 MPa). The modes of failure observed were (1) fabric/matrix debonding for carbon-FRCM; (2) debonding at the FRCM/concrete interface for the PBO-FRCM, and (3) premature fabric failure for glass–FRCM systems. For the fabric debonding failure mode, the stress–slip curves started with almost zero slip up until a threshold stress value, after which the fabric slippage began and progressed to failure. For the FRCM/concrete debonding, the stress–slip curves remained linear until (sudden) failure.

Bellini et al. (2019) performed single-lap shear tests on six different FRCM types (two carbon fiber meshes, two glass fiber meshes, aramid and basalt fiber meshes embedded in lime mortar) applied on masonry substrate. Both monotonic test and cyclic test (5 cycles at 25%, 50%, 75% of the average peak load) were carried out. Evident slip variation was noted between the first and the second cycle, with a progressive attenuation among cycles. Bond degradation in general did not prevent to reach the monotonic envelop during the following loading phase. They have concluded that the cyclic loading seemed to have negligible influence on the maximum bond capacity.

In addition to the bond test, the lap-splice length of the FRCM system was also investigated by Arboleda et al. (2016), Donnini et al. (2019a), D'Ambrisi et al. (2013), Nadianjav et al. (2021) and Orchirbud et al. (2020). Arboleda et al. (2016) investigated the splice length of PBO-FRCM and C-FRCM. When Arboleda et al. (2016) used a clamping grip for the C-FRCM and PBO-FRCM, the failure mode was slippage of the fabric between the two layers from the coupon center. The results indicated that a length of overlap equal to 100 mm was not sufficient to guarantee a proper stress transfer for the system tested. When using a clevis grip, they suggested a minimum overlap length of 150 mm for a PBO-FRCM.

Donnini et al. (2019a) investigated the overlap length of a single layer of glass fabric using the clevis grip. They have concluded that the overlap length up to 150 mm allowed to restore specimen's integrity and to reach an ultimate stress equal to that of the specimen with continuous fabric. It is noted that Donnini et al. also implemented a variational formulation on a finite element code and simulated the tensile behavior of the FRCM system and the effects of using different fabrics' overlap lengths.

The knowledge on the basic mechanical characteristics of the FRCM system such as the tensile behavior and the bond characteristics including the overlap length or the splice length can be utilized to investigate the behavior of the concrete columns laterally confined by the FRCM system. Donnini et al. (2019b) used a single carbon fabric with an overlap length of 150 mm to confine low strength (about 12 MPa) concrete cylinders. Both low-strength (15 MPa) and normal-strength (45 MPa) mortars were used along with the carbon fabric. The FRCM confinement was effective to demonstrate significant gain in strength (18–25%) and ductility (34–63%) while all test results showed strain-softening behaviors. No substantial differences in the peak load were noticed by changing the mortar strength class. Failure mode was by fibers slippage and breakage after the formation of several longitudinal cracks on the mortar surface. Gonzalez-Libreros et al. (2019) used C-FRCM to confine low strength concretes (about 17 MPa). When two layers of carbon fabric were used to confine concrete cylinders with 150-mm overlap length, a hardening behavior for the confined concretes was observed. The strength gain was 33% while the ultimate strain increased to 3.33 times that of the unconfined concrete cylinder.

In all studies summarized above, the FRCM systems were constructed by the wet layup technique (or the manual impregnation technique). In the wet layup method, a thin layer of mortar (about 3–5 mm) is first applied on top of roughened surface of existing concrete using hand trowel and then a fabric layer is gently pushed into the mortar followed by application of the second mortar layer of the same thickness. For the application of more than one FRCM layer, the last two processes are repeated. The FRCM system is then cured for a predetermined period. In this study, a new method of implementing the FRCM system for the concrete column strengthening is considered in a form of prefabricated FRCM system. Thin light-weight FRCM circular or flat panels can be fabricated in the laboratory/shop and brought to the site of application. The prefabricated FRCM panels can be assembled/installed in the field. As needed, the gap between the panels and the existing concrete is filled by high flowing mortar where the prefabricated FRCM panels serve as permanent formwork. Advantages of the prefabricated FRCM system include the following:

(1) A FRCM technology with increased constructability;
(2) Improved quality control which leads to improved durability; and
(3) Chance for more intensive strengthening by providing relatively large amount of fabric in the matrix.

In this study, authors' work consists of three steps of experimental research: tensile test of C-FRCM system was first performed to develop clear understanding of the mechanical behavior in tension; Secondly, lap-splice length of the C-FRCM was evaluated by conducting splice test in tension and interpreting the test data; Finally, small concrete columns were confined by prefabricated C-FRCM and the uniaxial behavior of the confined columns were investigated.

2 Material Properties and Preparation for Test

2.1 Materials

2.1.1 Carbon Fabrics

Two different carbon fabrics were used: A bonded fabric which was manually made in the laboratory and a commercial woven fabric. Both fabrics consisted of high-strength carbon fiber rovings (12K). Mechanical properties of the carbon fiber (CF) roving used to fabricate the bonded fabric as well as those of the commercial woven fabric were tested following ISO 10406-2 (2015) using a 50-kN capacity Universal Testing Machine (UTM) with results as summaized in Table 1. The woven fabric can stretch and straighten and demonstrate a little larger rupture strain and lower strength and elastic modulus than the bonded fabric in Table 1. The bonded fabric consists of a CF roving at 15 mm o.c. in the axial direction (warp) and at 30 mm o.c. in the lateral direction (weft) as shown in Fig. 2a. The fiber rovings are bonded together using an adhesive at each junction. The mass of the fabric is 81.7 g/m^2. For the woven fabric, the axial fibers consist of double CF rovings spaced at 25 mm o.c. and the lateral fibers consist of a single CF roving spaced at 20 mm o.c., respectively. The mass of the woven fabric is 106 g/m^2.

2.1.2 High-Strength Green Mortar

Use of recycled materials in concrete is becoming more important for cyclic economy. A high-strength green mortar was developed in part of an ongoing research on high-performance concrete using recycled fine aggregates and recycled fines. The specific mix used incorporated 100% recycled fine aggregate with the maximum particle size of 2.5 mm. Waste glass powder (≤ 40 μm) produced by finely grinding the waste glass bottles was also utilized to substitute 16% of the binder by mass. Polycarboxylate superplasticizer was used to control the mortar flow. For the tensile and the lap-splice tests, the mortars were cast and continuously wet cured until the test dates. Average compressive strength was determined by testing three 50 mm × 50 mm × 50 mm cubes while the flexural strength was determined by testing three 40 mm × 40 mm × 160 mm mortar prisms under three point bending. ACI 549.4R (2013) requires that the void content and the drying shrinkage of the mortar be determined. The void content was determined following ASTM D642 after 28 days. The shrinkage of the mortar bar specimen was measured in an environmental chamber ($T = 20 \pm 2$ °C, R.H. $= 60 \pm 5$%). Three prismatic bar specimens were demolded after 24 h and then immediately brought into the environmental chamber for the shrinkage measurement that continued for 90 days.

For the column confinement test, the C-FRCM test specimens were cast and demolded after 24 h. Then the specimens were mild heat cured for 48 h in an environmental chamber where the temperature (T) was 55 ± 3 °C and the relative humidity (R.H.) was 60 ± 5%. The high-strength green mortar (HM-RFA) was alweays used for the C-FRCM. For Type-3 column confinement tests, the high-flowing mortar using natural sand (HM-NFA) was used as filler mortar as needed (See Clause 2.2.3). The HM-NFA was basically the same mix as the HM-RFA except that the natural sand was used rather than the recycled sand as shown in Table 2. Superplasticizer was used to control the flow of the mortars as shown in Table 2.

Table 1 Mechanical properties of carbon fabrics.

Fabric type	Strength		Strain at peak		Elastic modulus		Applied to
	Average (MPa)	COV (%)	Average (%)	COV (%)	Average (GPa)	COV (%)	
Bonded fabric	2179	2.50	1.24	5.20	176	4.50	Tensile test; Lap-splice test
Woven fabric	1753	11.82	1.26	9.30	139	9.33	Column confinement

Average of ten tests for each type; density = 0.0018 g/mm^3 for carbon fiber, cross section (CF 12K) = 0.454 mm^2.

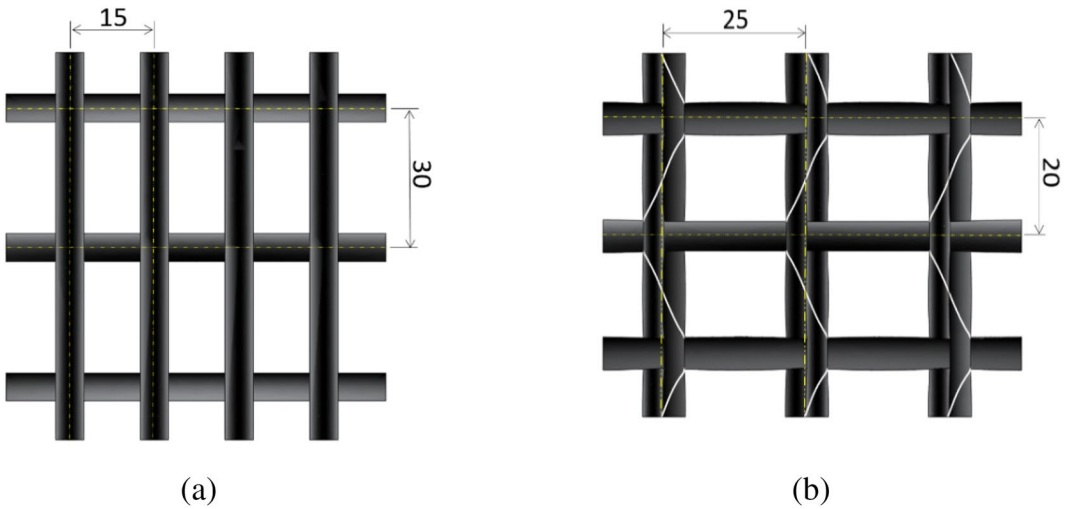

Fig. 2 Carbon fabrics made of CF 12K rovings: **a** laboratory-made bonded fabric used for tensile test and lap-splice test; **b** commercial woven fabric used for column confinement test.

2.2 Preparation for Test

2.2.1 Tensile Test

The C-FRCM system was constructed considering a prefabricated system in this study and so the wet-layup technique was not used. Fabrication of the tensile test specimens with one fabric layer was implemented in the following sequence: along perimeter of a stiff rectangular acrylic base panel, 5-mm-thick acrylic sections were first placed/bonded to the base panel. CF rovings were manually installed across the opposite acrylic sections both in the axial and the lateral directions. After the fabric installation was completed, another layer of 5-mm-thick acrylic sections was bonded on top of the existing sections. HM-RFA was cast at one time. For the tensile test specimens with two fabric layers, the installation sequence was the same as that used for the one fabric layer except that the second fabric layer was installed on top of the first layer. No intentional gap was introduced between the fabric layers while the two fabric layers were not bonded. As a result, the thickness of the panels with one fabric layer or two fabric layers was about the same (~ 10 mm).

Fresh mortar was consolidated for 1 min using a vibrating table. The specimens were continuously wet cured for 28 days. The FRCM panel dimensions were 405 mm (b) × 450 mm (h) x ~ 10 mm (t). After 28 days, the FRCM panel was cut using waterjet and nine 45-mm wide, 450-mm long, and about 10-mm thick prismatic bars were retrieved. Two bars recovered from both sides of the panel were used for preliminary test. As a result, a total of seven tensile test specimens were prepared. One week prior to testing, a set of two 6-mm-thick steel tabs (40 mm × 200 mm, bond length = 165 mm) was bonded to each end of the tensile test specimen using a two-part epoxy as shown in Fig. 3. A predrilled hole at the extremity of the steel tabs allowed a pin connection to the 8-mm-thick rectangular steel plate which was then connected to the hydraulic grips of the UTM during test. The test setup shown in Fig. 3 allows a rotational degree of freedom at each end while the fibers are free to slip inside the mortar similar to the clevis grip. The behavior of 120-mm mid length was monitored during tensile test. The tensile tests were performed under displacement control at a rate of 1 mm per minute using Instron 4495 UTM

Table 2 Mortar mix design for 1 m^3 and flow, void ratio and shrinkage properties.

Mortar	C (kg)	SF (kg)	WGP (kg)	Sand (kg)	W (kg)	w/b	Flow (cm)	Void ratio (%)	$\varepsilon_{shr\,90d}$ (μm/m)
HM-RFA	550	27.5	110	1487	206	0.3	24.2	17.6	694
HM-NFA	530	26.5	106	1573	190	0.3	22.5	–	–

C: cement; SF: silica fume; WGP: waste glass powder; RFA: recycled fine aggregate (≤ 2.5 mm); NFA: natural fine aggregate (≤ 2.5 mm); polycarboxylate superplasticizer 1% and 2% of binder by mass for HM-RFA and HM-NFA, respectively; small amount of defoaming agent is used; Mortar flow was determined following KS L 5105; Void ratio was determined following ASTM D642; $\varepsilon_{shr\,90d}$: total shrinkage after 90 days.

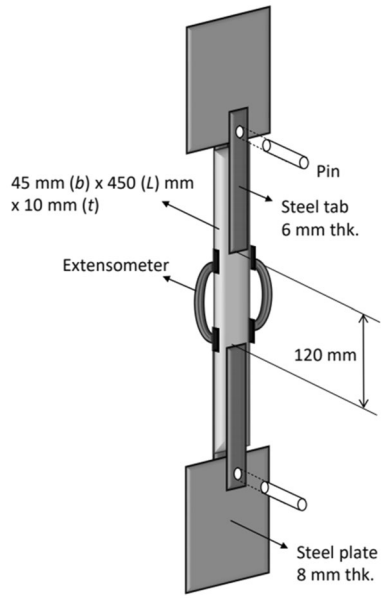

Fig. 3 Tensile test setup.

with 1200-kN capacity. The accuracy of the UTM load cell was verified during preliminary test for use of a relatively large capacity UTM for the tensile test. A set of extensometers with 100-mm gauge length was used to measure axial strains developed at center as shown in Fig. 3. In addition, a set of linear variable displacement transducers (LVDTs) was used to monitor the movement of the UTM crosshead (see Fig. 7a). All electronic signals were monitored during test and recorded using a data logger and a notebook computer.

2.2.2 Lap-Splice Test in Direct Tension

The lap-splice test was conducted to determine the minimum splice length for the lateral confinement of concrete columns by the prefabricated C-FRCM. The lap-splice test specimens were made in a fashion similar to the tensile test specimens. Along perimeter of a rectangular base panel, 5-mm-thick acrylic plates were placed/bonded to the base panel. The bonded carbon fabrics were manually installed in a similar fashion to the tensile specimens. The splices are located at center as shown in Fig. 4. Two fabrics are spliced for a single lap-splice test as shown in Fig. 4a. For the double lap-splice test, two sets of spliced

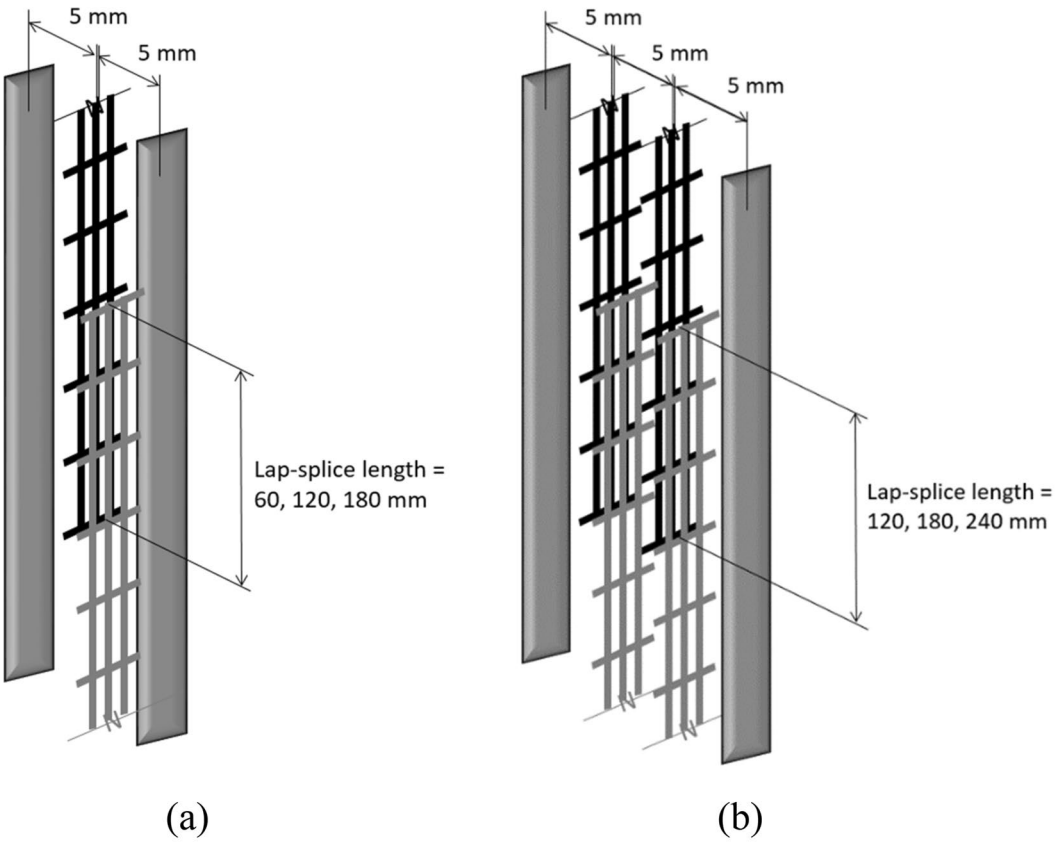

Fig. 4 Lap-splice test specimen: **a** single lap-splice, **b** double lap-splice.

fabrics are used with 5-mm spacing between two different sets of the fabric layers as shown in Fig. 4b. The HM-RFA was cast at one time after completion of the fabric installation. The C-FRCM panels were continuously wet cured for 28 days and then six 45-mm-wide and 450-mm-long thin prismatic specimens were cut out from the panel using waterjet. Average thickness of a single lap-splice specimen was 13.7 mm. The average thickness of a double lap-splice specimen was 19.4 mm. Three different splice lengths were tested: 60 mm, 120 mm, 180 mm for the single lap-splice test and 120 mm, 180 mm, and 240 mm for the double lap-splice test. Two replicate specimens were tested. The tensile test setup shown in Fig. 3 was used for the lap-splice test in direct tension.

2.2.3 Lateral Confinement of Columns by C-FRCM

Commercial woven fabrics (see Fig. 2b) were used for this part of the experimental program. Six FRCM-confined plain concrete cylinders or prisms consisted of three types: (Type-1) concrete cylinder was confined by C-FRCM with an overlapped fabric; (Type-2) concrete cylinder was confined by C-FRCM with lap-spliced fabrics; (Type-3) concrete prism was confined with a prefabricated C-FRCM tube with lap-spliced fabrics. Three different cross-sections are shown in Fig. 5.

Vertical surface of the plain concrete cylinders (diameter = 150 mm, height = 300 mm) or prisms (100 mm × 100 mm × 300 mm) was lightly ground using a hand grinder. The treated surface was cleaned by compressed air and dampened using wet towels before casting. For Type-1 confinement (i.e. cylinder + fabric overlap), a sufficient length of the carbon fabric was used to provide an overlap length equal to about one-half the perimeter length as shown in Fig. 5a. For Type-2 and Type-3 confinement (i.e. cylinder or prism + lap-spliced fabrics), the lap-splice length was 170 mm as shown in Fig. 5b and c. Steel wires were used to tie the overlapped or lap-spliced fabrics. For Type-1 and Type-2 confinement tests, the fabrication procedure of the test specimens was as follows: (1) inside an acrylic cylindrical mold with 180-mm inner diameter, a concrete cylinder was placed at center; (2) preassembled carbon fabric(s) was placed in the gap between the acrylic mold and the concrete cylinder; and (3) the gap was filled by the HM-RFA. The specimens were consolidated for 1 min on a vibrating table. 24 h after casting, the specimens were demolded and brought into an environmental chamber and mild heat cured for 48 h. Test began 7 days after the in situ casting of the C-FRCM. For the Type-3 confinement test, 15-mm-thick FRCM tubes with 180-mm outside diameter were first fabricated and heat cured for 72 h. The FRCM tubes were cooled down and stored in room temperature for four days. A concrete prism was placed at center inside the prefabricated FRCM tube. High-flowing mortar (HM-NFA) was cast to fill the gap between the prefabricated FRCM tube and the concrete prism without introducing any consolidation, which was then continuously wet cured for 7 days. Test began 7 days after casting the filler mortar (i.e. 2 weeks after fabrication of the FRCM tube).

Uniaxial compression tests were performed under displacement control with a ramp rate of 0.1 mm/min using a 3000-kN-capacity compression testing machine. Special compressometer equipped with eight LVDTs was used (i.e. a set of four LVDTs was used to measure the axial deformation and another set of four LVDTs was used to measure the lateral displacement) to measure displacements. In addition, two pairs of 30-mm-long electronic strain gauges (a pair in the vertical direction and the other pair in the horizontal direction, respectively)

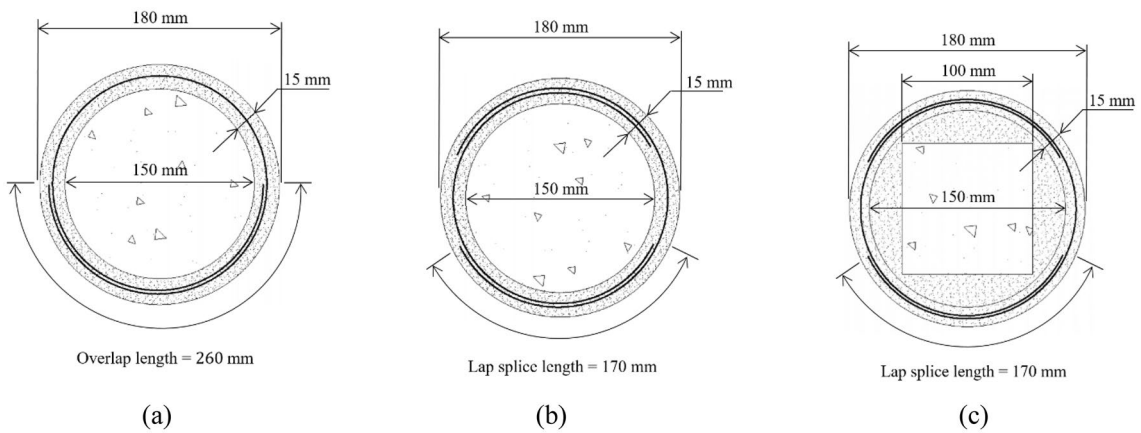

Fig. 5 Confinement test: cross sections of circular specimens. **a** Type-1, **b** Type-2, **c** Type-3.

Fig. 6 Confinement test: a prism confined by FRCM tube with lap-spliced fabrics. **a** Fabrication of lap-spliced fabrics; **b** prism and C-FRCM tube before casting filler mortar; **c** test under progress.

were bonded to the face of the specimen at 180° angle to each other as shown in Fig. 6c. Two replicate specimens were tested per test type.

3 Test Results

3.1 Mechanical Properties of Mortars

For continuously wet-cured high-performance mortar with recycled fine aggregate 1, RFA1 (HM-RFA-MC-1, -2), the average compressive strength is 71.3/78.6 MPa. The compressive strength is significantly lower 51.2 MPa after 28 days for HM-RFA-MC-3 which used RFA-2 (see note to Table 3). For the moderate heat-cured recycled aggregate mortar (HM-RFA-HC-3), the compressive strength is 52.4 MPa after 28 days.

3.2 Tensile Test Results

The tensile test results are summarized in Table 4 in terms of specimen width, thickness, cracking load, ultimate load as well as displacement at the cracking load and at the maximum load. The specimen index is as follows: CF—carbon fabric; T1 or T2—tensile test of C-FRCM with one fabric or two fabrics; 1 through 7—replicate number. Figs. 8 and 9 show the stress-versus-strain plots determined from the tensile tests of the C-FRCM with one and two layers of fabric, respectively. From seven tensile tests of the C-FRCM with one fabric layer, the average nominal stress of the composite section at cracking (i.e. cracking load divided by gross area) was 2.59 MPa (see Fig. 7b). As the load increased, the number of cracks increased as shown in Fig. 7c. The tensile cracks typically appeared at the position of the lateral fibers due to the reduced mortar cross section. After the number of cracks reached the maximum of 3–5 cracks, no new cracks appeared, but the existing cracks widened. Close to the peak load, the width of a single dominating crack increased fast while the width of the other cracks decreased. Significant local slip of the fibers from the mortar was evident adjacent to a wide crack as shown in Fig. 7d. All fibers ruptured in tension at the peak after which the resistance of the C-FRCM was lost immediately as shown in Fig. 8. The amount of the axial fibers provided was 0.30% by vol. The tensile test results showed a

Table 3 Summary of mortar strength development.

Mortar	Compressive strength (MPa) and COV (%)						Flex. strength (MPa) at 28 d		Remarks
	7 d	COV	28 d	COV	56 d	COV	f_r	COV	
HM-RFA-MC-1	55.8	1.86	71.3	3.36	75.6	6.80	5.50	14.6	Tensile test
HM-RFA-MC-2	67.0	2.33	78.6	3.70	85.3	4.08	–	–	Splice test
HM-RFA-MC-3	31.1	4.60	51.2	6.41	–	–	–	–	Column test
HM-RFA-HC-3	44.4	1.20	52.4	3.85	–	–	–	–	FRCM tube
HM-NFA-MC	55.3	3.02	–	–	–	–	–	–	Filler mortar

Average of three tests; two different recycled fine aggregates were used (RFA1: $BSG_{SSD} = 2.52$, water absorption = 2.34%—used for HM-RFA-MC-1, -2; RFA2: $BSG_{SSD} = 2.50$, water absorption = 2.63%—used for HM-RFA-MC-3, -HC).

Table 4 Summary of tensile test results: CF 1 layer and CF 2 layers.

Index	*w* (mm)	*t* (mm)	P_{cr} (kN)	P_{max} (kN)	Displ. @ P_{cr} (mm)	Displ. @ P_{max} (mm)	No. of cracks	Failure mode
CF-T1-1	44.15	9.55	1.67	3.37	0.30	1.88	5	FR
CF-T1-2	44.15	10.15	1.08	3.78	0.13	1.88	5	FR
CF-T1-3	44.15	10.55	0.72	3.58	0.13	1.88	4	FR
CF-T1-4	44.05	11.05	1.37	3.38	0.16	1.72	4	FR
CF-T1-5	44.15	11.85	1.30	3.43	0.26	1.70	3	FR
CF-T1-6	44.05	11.55	1.36	3.53	0.24	1.99	5	FR
CF-T1-7	44.15	11.05	1.15	3.65	0.17	2.37	5	FR
Average	44.12	10.82	1.236	3.531	0.197	1.916		
Stdev	0.049	0.799	0.295	0.151	0.066	0.225		
CF-T2-1	44.15	10.55	2.69	6.44	0.16	2.68	4	FS
CF-T2-2	44.45	11.65	0.92	5.98	0.12	2.02	4	FS
CF-T2-3	44.15	11.85	2.53	5.45	0.38	1.69	4	FS
CF-T2-4	44.65	12.55	2.84	6.11	0.21	2.28	5	FR
CF-T2-5	44.45	12.65	2.90	5.77	0.37	1.94	4	FS
CF-T2-6	44.15	12.35	2.16	5.14	0.14	1.94	3	FS
CF-T2-7	44.05	11.85	1.19	5.66	0.23	2.03	5	FS
Average	44.29	11.92	2.176	5.793	0.228	2.08		
Stdev	0.223	0.716	0.807	0.431	0.106	0.315		

P_{cr} is cracking load; P_{max} is ultimate load; Displ @ P_{cr} is displacement at cracking; displ. @ P_{max} is displacement at P_{max}; Failure mode FR is fiber rupture while failure mode FS is fiber slip from mortar.

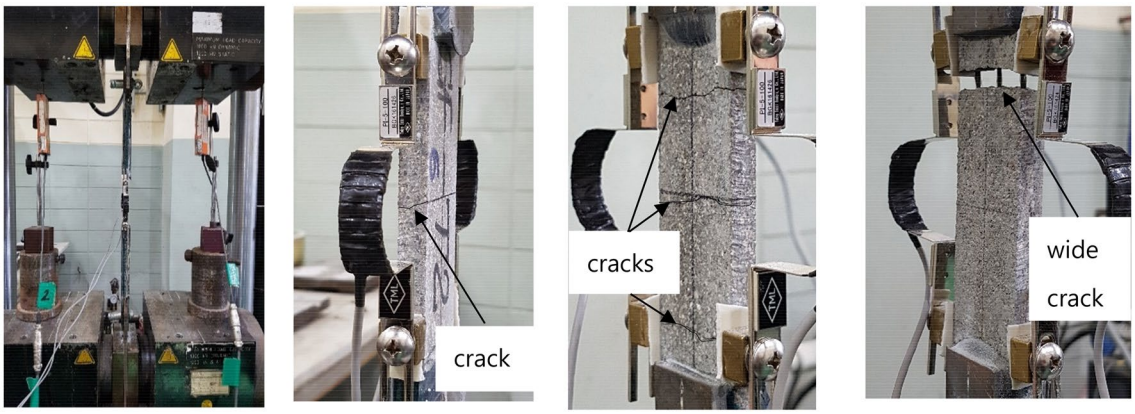

Fig. 7 Tensile test on FRCM composites: **a** test setup, **b** at cracking, **c** multiple cracks, **d** a dominant crack.

brittle behavior with resistance equal to 7.40 MPa (nominal stress: i.e. peak load divided by gross area) at ultimate while the average fiber stress is 2593 MPa at 1.6% tensile strain on average as shown in Table 5 and Fig. 8.

From all tensile tests of the C-FRCM with two layers of fabric, the average nominal stress was 4.12 MPa at the first cracking. At the maximum load, the average nominal stress was 11.0 MPa. The fiber stress at ultimate is 2127 MPa on average at 1.73% strain as shown in Table 5 and Fig. 9. After the peak, the resistance of the C-FRCM with two layers of fabric is significantly reduced as the fibers slip from the mortar. The C-FRCM still resists about 20% or more of the peak load (except for CF-T2-4 where all fibers ruptured) as shown in Fig. 9. Test ended when the displacement was 3 mm or greater. The tensile test results indicated a pseudo-ductile behavior associated with the multiple cracking and the slip between the fibers and the mortar when the axial fiber amount of 0.59% by vol. was used.

Table 5 Summary of tensile test results.

	f_{cr}		ε_{cr}		E_f^*		f_{fu}		ε_{fu}		E_f	
	Mean (MPa)	COV (%)	Mean (%)	COV (%)	Mean (GPa)	COV (%)	Mean (MPa)	COV (%)	Mean (%)	COV (%)	Mean (GPa)	COV (%)
CF-T1	907	23.9	0.065	37.7	1493	28.5	2,593	4.30	1.60	11.7	85.6	12.2
CF-T2	799	37.1	0.082	49.8	1034	31.8	2,127	7.44	1.73	15.1	93.1	25.1

Average of 7 tests; f_{cr}—axial fiber stress at the first cracking; ε_{cr}—axial strain at the first cracking; E^*—slope of the line of the stress–strain plot connecting the origin and the cracking point; f_{fu} – axial fiber stress at ultimate; ε_{fu}—axial strain at ultimate; E_f – stiffness of C-FRCM determined using Eq. (1).

In all tensile tests, the full fiber strength in tension is reached in the current C-FRCM as summarized in Table 5. Test results also indicate that the current test setup properly allows the fibers to slip from the mortar without inducing any significant bending moment. It is noted that, the measured strains by the extensometers showed variation. Because the extensometer length of 100 mm did not cover the entire 120-mm length between the steel tabs, some cracks formed outside the gauge length of the extensometers. Therefore, the displacement readings from the LVDTs were used to summarize test results in Table 4 (since the stiffness of the steel tab was much greater than that of the C-FRCM, the measured displacements were safely assumed to have occurred in the mid 120-mm length). The extensometer readings were used to summarize the tensile test results of Table 5. In Table 5, the average cracking load of the C-FRCM with two fabric layers is lower than that for the C-FRCM with one fabric layer because the mortar section is reduced by the larger amount of the fibers. At ultimate, as the two fabrics in the axial direction are on top of each other with little spacing in the current prefabricated C-FRCM and thus have smaller chance of impregnation by the mortar, the fiber stress at the maximum load is lower than that for the C-FRCM with one fabric layer. The C-FRCM with two fabric layers also slips a little more than the C-FRCM with one fabric layer on average as demonstrated by the ultimate fiber strain ε_{fu}. The stiffness E_f is relatively high for the C-FRCM with the two fabric layers indicating that the behavior is more dependent on the fibers. In Table 5, E_f was determined based on strain and stress readings at two points of the stress–strain curves corresponding to $0.6f_{fu}$ and $0.9f_{fu}$ by Eq. (1) as recommended by ACI 549.4R (2013):

$$E_f = \frac{0.9f_{fu} - 0.6f_{fu}}{\varepsilon_{f@0.9f_{fu}} - \varepsilon_{f@0.6f_{fu}}}, \tag{1}$$

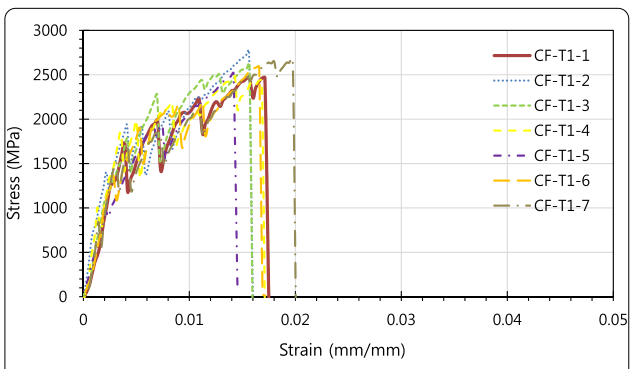

Fig. 8 Tensile test results: C-FRCM with one layer of fabric.

where $\varepsilon f@0.6f_{fu}$ and $\varepsilon f@0.9f_{fu}$ represent fiber strains at 0.6 f_{fu} and 0.9 f_{fu}, respectively.

3.3 Lap-splice test results

Tests were performed in direct tension for the lap-splice test specimens with a set of single fabrics or double fabrics spliced at center to determine the minimum splice length. The splice length was 60 mm, 120 mm, 180 mm for the single lap-splice tests and it was 120 mm, 180 mm, 240 mm for the double lap-splice tests. Two replicate specimens were tested. The test results are summarized in Table 6. The specimen index is as follows: CF—carbon fabric; S1 or S2—single splice or double splice; 60, 120, 180, 240—splice lengths in mm. Stress-versus-strain plots for the single lap-splice tests and the double lap-splice tests are shown in Figs. 11 and 12, respectively. With increasing load, the first two cracks typically formed close to both ends of the splice as shown in Fig. 10a probably due to changes in the cross-sectional geometry and the bending moment induced by asymmetric fiber configuration at the end of the splice (Donnini et al. (2019a) analytically demonstrated that the first cracks form at the ends of a splice). For specimens with a short splice length of 60 mm, the number of cracks did not increase, but the existing cracks widened with increasing load indicating significant slip between the fibers and the mortar (see Fig. 11: CF-S1-60-1). At the ultimate, all axial fibers ruptured at the end of the splice (see Fig. 10b). When the splice length was 120 mm, the first crack also formed at the end of the splice as shown in Fig. 10c. The number of cracks increased with increasing load as shown in Fig. 10d. At ultimate, the fibers ruptured at an end of the splice of CF-S1-120-1 (see Fig. 11). With the splice length of 180 mm, the cracking and the stress–strain behaviors were similar to those of the specimens with 120-mm splice length in general, but tests resulted in much higher maximum stresses and strains as shown in Fig. 11: CF-S1-180-1, -2. The maximum stress-versus-splice length plots of all single lap-splice tests are shown in Fig. 13a. It is shown that the maximum stresses are approximately proportional to the splice lengths and the minimum splice length can be determined as a result of the linear regression of the test results, which is 168 mm (about 170 mm). The current conclusions can be backed up by the fact that the stress–strain plots, peak stress, strain at the peak, and elastic modulus of the lap-splice test specimens with 180-mm splice length as shown in Fig. 11 and Table 6 match well those of the tensile test results of the C-FRCM with one continuous fabric layer in Fig. 8 and Table 5.

The test results of the C-FRCM with double lap-splices in Table 6 and Fig. 12 also show that both maximum stresses and the strains at the maximum stress increase with increasing splice length which varies from 120 to 240 mm. The average maximum stress of 162 MPa determined from two specimens with the largest splice length (CF-S2-240-1, -2) are significantly smaller than the strength of CF 12K (2179 MPa in Table 1) despite significant slip indicated by the strain at the peak which is well over the rupture strain of CF 12 K. Test results indicate that the splice length of 240 mm is not sufficient for the specimens with double lap-splices. The maximum stresses-versus-splice length plots of all double lap-splice tests are shown in Fig. 13b. The minimum splice length can be determined as a result of linear regression of the test results, which is 308 mm (about 310 mm).

3.4 Behavior of Columns Laterally Confined by C-FRCM

Three different types of confinement scheme were used: (1) cylinders confined by cast-in situ C-FRCM with overlapped fabric, Type-1; (2) cylinders confined by cast-in situ C-FRCM with lap-spliced fabrics, Type-2; and (3) prisms confined by prefabricated C-FRCM tubes with high-flowing filler mortar in between the prism and the tube, Type-3. Two replicate specimens were tested per type. In addition, three cylinders and three prisms were also tested under compression as control specimens.

Test results are summarized in Table 7 and Figs. 14 and 15. From all uniaxial test of plain concrete cylinders or prisms laterally confined by C-FRCM, both enhanced strength and strain values at the peak load were observed. The strength gain was between 9.9–40.7% (28.1% for Type-1, 40.7% for Type-2, 9.9% for Type-3). Strains at the peak also increased over that of the control specimens by 6.0–44.9% (6.0% for Type-1, 32.4% for Type-2, 44.9% for Type-3).

All specimens showed the strain-softening behavior. A theoretical model by Mander et al. (1988) was used to compare the theoretical and the experimental behaviors in Figs. 14 and 15, where the theoretical stress–strain behaviors predicted by Mander et al. agree well with the actual behavior.

$$f_l = \frac{2E_f \varepsilon_h t_f}{D}, \tag{2}$$

where E_f is elastic modulus of fiber, t_f is thickness of fiber and D is diameter of cylinder surrounded by fiber (fiber center-to-center dimension).

In Table 7 and Fig. 14, both Type-1 and Type-2 specimens show similar stress–strain behaviors while Type-2 specimens show a little higher peak stresses and higher strains at the peak compared to those of Type-1 specimens. This is because the significant length of the perimeter of a cylinder is actually surrounded and confined by

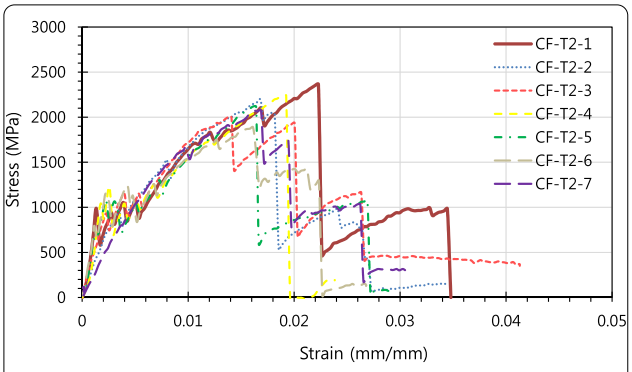

Fig. 9 Tensile test results: C-FRCM with two layers of fabric.

double fabrics due to employed lap-splice scheme (splice length of 170 mm × 2 = 340 mm) in the Type-2 specimens in comparison to the overlap length of about 260 mm of the Type-1 specimens (see Fig. 5). The peak load also increases significantly due to enlarged cross-section: The average peak loads are 184% and 208% of that of the control cylinders, for Type-1 and Type-2 specimens, respectively. Fig. 16 shows the crack patterns after test. Multiple vertical cracks in the axial direction typically develop at the end of the splices or the overlap as shown in Fig. 16a and b where the end of the overlap or the splice is marked using an arrow.

In Table 7 and Fig. 15a, for the Type-3 specimens where a plain concrete prism is surrounded by the C-FRCM tube and the gap between the prism and the tube is filled by the filler mortar, the strength gain is small (i.e. about 10% on average) while the average strain at the peak increases by about 45%. It is seen in Fig. 16c that the prefabricated C-FRCM tube debonded from the filler mortar. It should be noted that, after the fabrication of the C-FRCM tube, the inner surface of the tube was not roughened which must have caused early debonding between the prefabricated C-FRCM tube and the filler mortar. As the cross section is only partially composite, the efficacy of the

Table 6 Summary of lap-splice test results.

Index	P_{cr} (kN)	P_{max} (kN)	Displ. @ P_{cr} (mm)	Displ. @ P_{max} (mm)	f_{fu} (MPa)	ε_{fu} (%)	E_f (GPa)	No. of cracks	Failure mode
CF-S1-60	2.67	3.22	0.263	0.741	1183	0.62	n/a	2/2	FR-es
CF-S1-120	2.51	3.85	0.292	0.955	1416	0.80	99.1	4/5	FR-es
CF-S1-180	2.70	6.28	0.218	1.599	2304	1.33	99.1	5/5	FR-ms
CF-S2-120	2.75	5.35	0.227	1.105	983	0.92	75.5	3/4	FS-ms
CF-S2-180	2.83	7.46	0.161	1.741	1370	1.45	79.3	4/5	FS-ms
CF-S2-240	3.10	8.51	0.147	1.843	1562	1.54	85.1	5/5	FS-ms

Average of 2 tests; FR-es: fiber rupture at the end of splice; FR-ms: fiber rupture in the mid splice length.

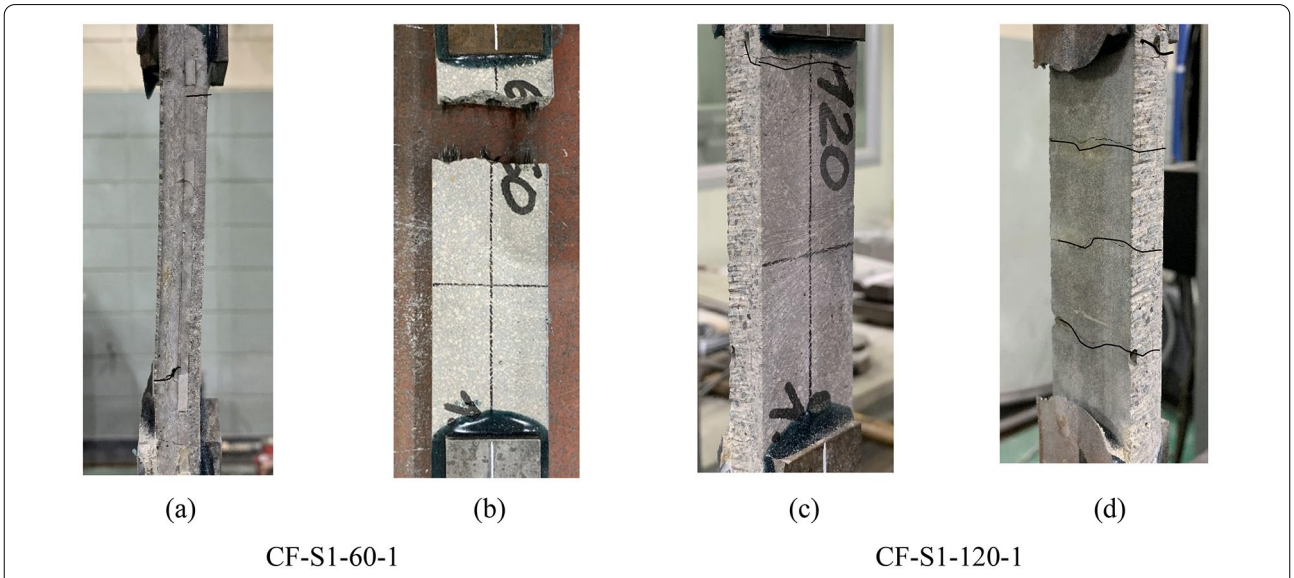

Fig. 10 Lap-splice test: crack and failure patterns. **a** Cracking, **b** failure, **c** cracking, **d** multiple cracks.

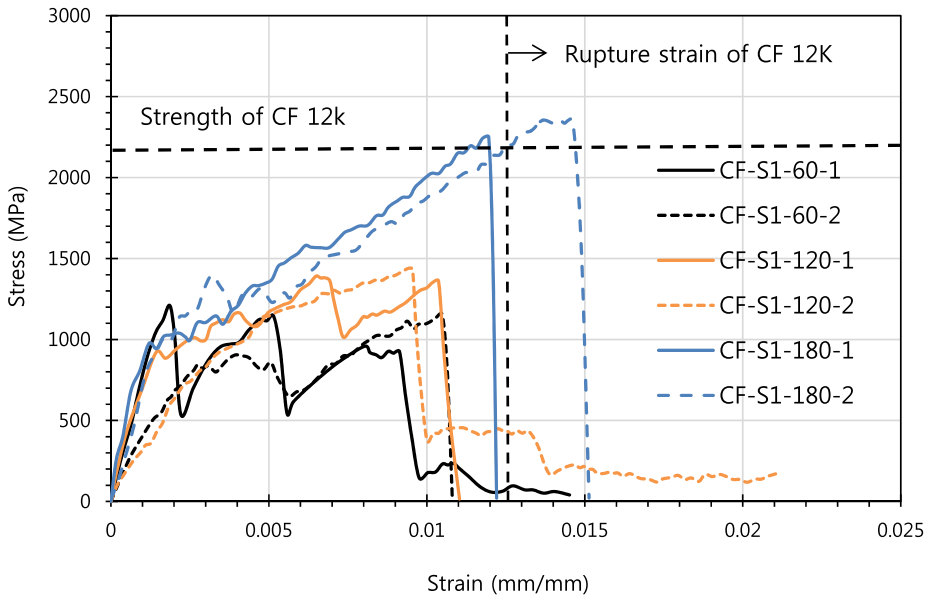

Fig. 11 Stress vs. strain: single lap-splice test results.

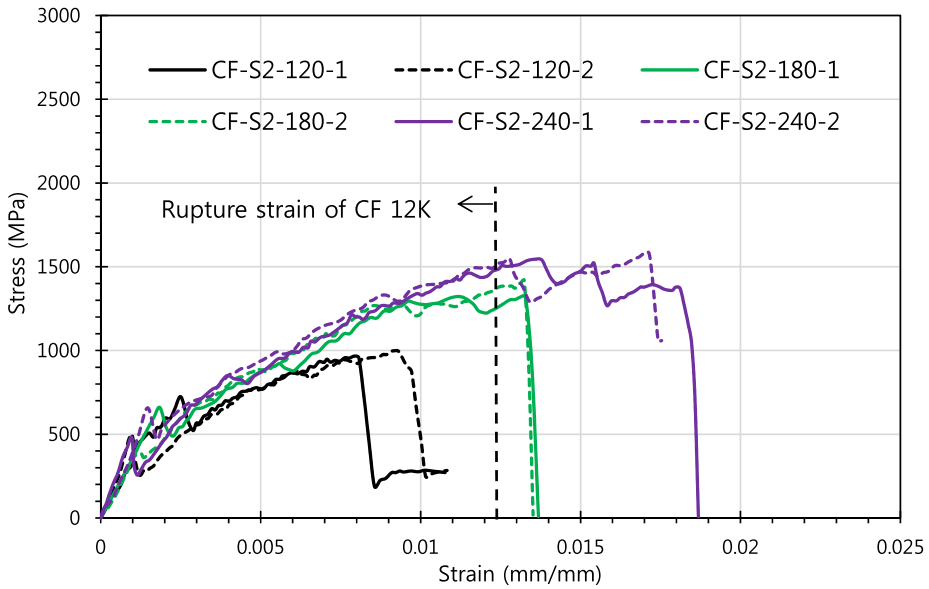

Fig. 12 Stress vs. strain: double lap-splice test results.

resistance mechanism was affected. On the other hand, in Fig. 15b, the gain in the load resisting capacity is very large due to significantly increased cross-section of the Type-3 specimens overt that of the control prisms (see Fig. 5c): i.e. Average peak load of the Type-3 specimens is 282% of that of the control prisms. It is noted that the stiffness of the Type-1 and -2 specimens is higher than that of the control cylinders in Fig. 14. However, the stiffness of the Type-3 specimens is the same as that of the control prisms in Fig. 15a probably due to the partially composite behavior as described previously.

4 Discussion

For the tensile test results, ACI 549.4R (2013) recommends that the design parameters (i.e. characteristic values) be determined by deducting a standard deviation

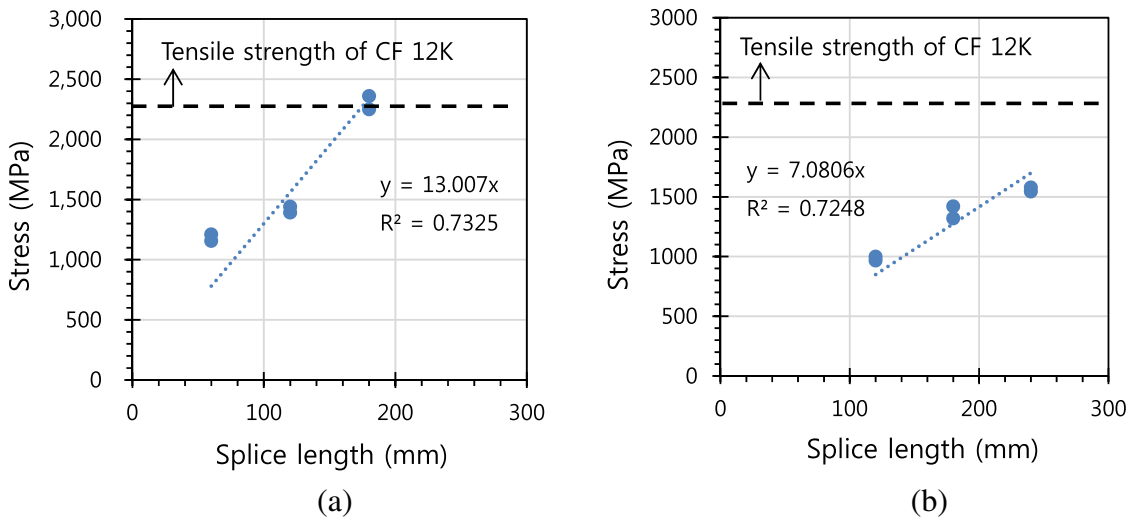

Fig. 13 Test results: lap-splice test. **a** Single lap-splice test, **b** double lap-splice test.

Table 7 Summary of test results: columns confinement by C-FRCM jacket.

Index	f'_{co} (MPa)	f'_{cc} (MPa)	ε_{co} (%)	ε_{cc} (%)	ε_h (%)	f_l (MPa)	k_1	P_{max} (kN)
C-1	28.58		0.157					505
C-2	28.85		0.188					510
C-3	28.52		0.200					504
Average	28.65		0.182					506
P-1	37.89		0.155					379
P-2	38.99		0.180					390
P-3	37.01		0.165					370
Average	37.96		0.167					380
C-OL-1		37.28		0.186	0.067	0.0872	98.9	948
C-OL-2		36.09		0.199	0.083	0.1080	68.8	918
Average		36.69		0.193	0.075	0.0976	83.8	933
C-S1-1		40.68		0.244	0.189	0.2461	48.8	1035
C-S1-2		39.96		0.237	0.184	0.2396	48.7	1074
Average		40.32		0.241	0.187	0.2428	48.7	1055
P-S1TB-1		42.86		0.246	0.200	0.2604	13.2	1053
P-S1TB-2		40.57		0.237	0.056	0.3086	8.45	1090
Average		41.72		0.242	0.128	0.2845	10.8	1072

f'_{cc} (or f'_{co}): P_{max}/gross area; ε_{cc} (or ε_{co}): strain at the peak; ε_h: hoop strain at the peak; f_l: lateral confinement pressure determined using Eq. (2).

from the mean values of the test results. The design parameters for the tensile strength and the ultimate strain as well as the elastic modulus of the C-FRCM system used in this study were determined as summarized in Table 8.

Current lap-splice test results show that the splice length of the double lap-spliced fabrics (310 mm) is significantly larger than that of the single lap-spliced fabrics (170 mm). Since the cover thickness of all specimens is the same (about 5 mm) in the single lap-splice and the double lap-splice tests (see Fig. 4), it is proposed that the splice length is also affected by the spacing between two adjacent fabric layers in a similar fashion it is affected by the cover mortar thickness. It is likely that the stiff and strong junctions of the bonded carbon fabric contribute to the mechanical performance of the fabric (Peled et al., 2009).

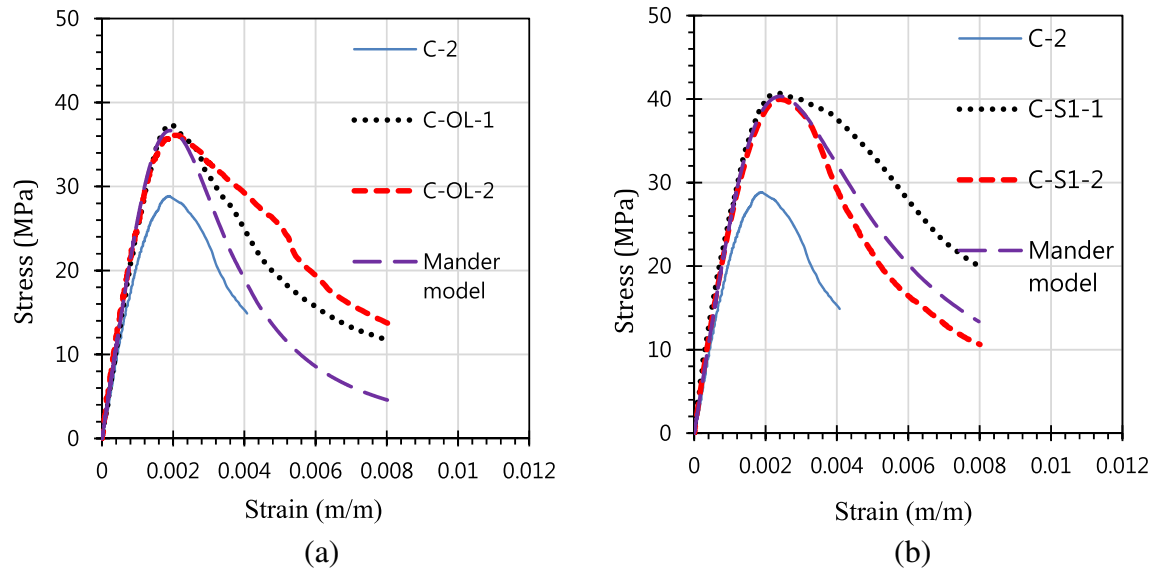

Fig. 14 Control specimen vs. Type-1 (overlap) and Type-2 (lap splice) cylindrical specimens. **a** Type-1: stress vs. strain; **b** Type-2: stress vs. strain.

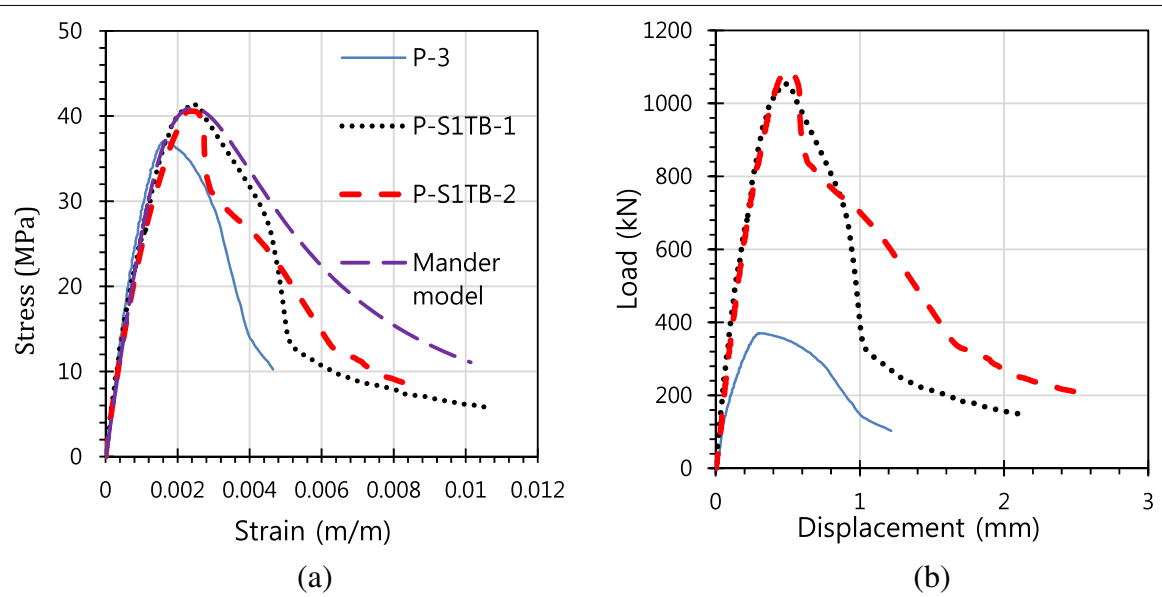

Fig. 15 Control specimen vs. prismatic specimens with FRCM tube (Type-3): **a** stress vs. strain, **b** load vs. displacement.

Three different types of uniaxial compression test of plain concrete columns have been conducted. The stress–strain behaviors of the Type-1 and Type-2 specimens were similar which corroborates that the splice length employed in this study (170 mm) is adequate. Debonding between the filler mortar and the prefabricated C-FRCM tube was noticed from Type-3 specimens after test. Due to debonding, benefit of the full composite action could not be achieved from the Type-3 specimens. However, it can be improved by roughening the inner surface of the C-FRCM tube. Test results of Type-3 specimens indicated applicability of the prefabricated type C-FRCM in the future. Finally, it must be noted that the current study is part of an on-going research on the applicability and the mechanical behavior of the prefabricated C-FRCM system. Larger specimens with lap-spliced carbon fabrics and prefabricated multi-segment C-FRCM panels are

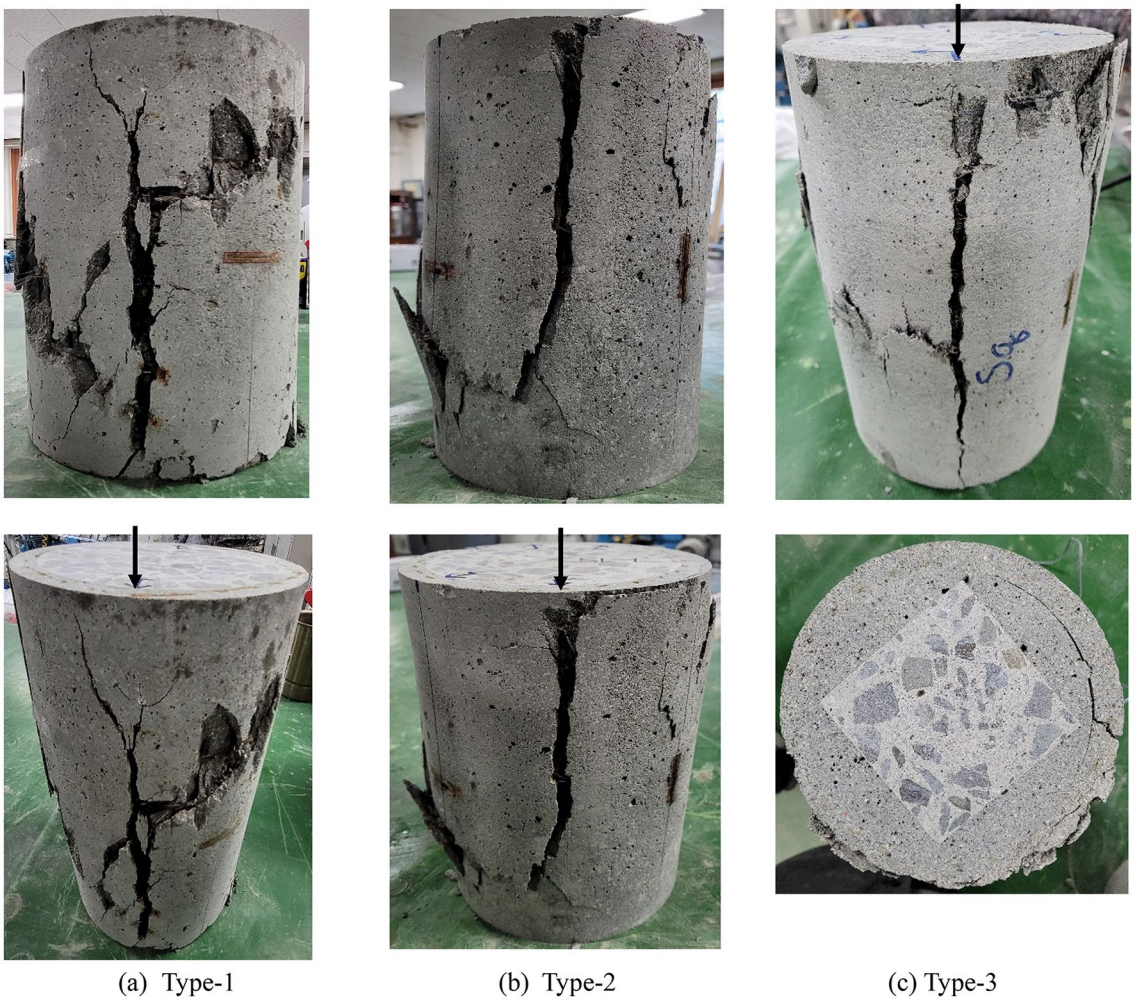

Fig. 16 Specimens after test: crack patterns. **a** Type-1, **b** Type-2, **c** Type-3

Table 8 Design parameters of C-FRCM in tension (ACI 549.41R).

Index	f_{fk} (MPa)	ε_{fk} (%)	E_f (GPa)
CF-T1	2,581	1.58	85.6
CF-T2	1969	1.70	93.1

characteristic strength (or strain) = mean – one standard deviation for (f_{fk} and ε_{fk}); Mean value is used for E_f as determined using Eq. (1).

being considered by the authors which can be applied in the field to existing RC columns.

5 Conclusions

Current study consists of three different experimental works: (1) test of C-FRCM in direct tension; (2) lap-splice length test in direct tension; and (3) uniaxial compression test of plain concrete cylinders and prisms laterally confined by cast-in situ or prefabricated C-FRCM. The following conclusions can be made from the current experimental study:

(1) Axial fiber volumetric ratio of 0.6% or greater is recommended for the C-FRCM to demonstrate a pseudo-ductile behavior in tension. Tensile tests of C-FRCM with 0.3% axial fiber by vol. showed a brittle behavior while the C-FRCM with 0.59% axial fiber by vol. resulted in a pseudo-ductile behavior.
(2) Full strength of the carbon fabric was developed in all tensile tests. With use of the green high-strength mortar, the nominal tensile strength was 7.4 MPa for the C-FRCM with one fabric layer and 11.0 MPa with two fabric layers in direct tension.
(3) Green high-strength mortar was used in this study that employed 100% recycled fine aggregate. 16% of the binder by wt. was also replaced by waste glass

powder. Overall mechanical performance of the C-FRCM utilizing the green high-strength mortar was satisfactory.

(4) Lap-splice length of the carbon fabrics was determined from linear regression of the test results as follows: 170 mm for the single fabric and 310 mm for the double fabrics.

(5) From six uniaxial compression tests of small plain concrete cylinders or prisms confined by one layer of carbon fabric, the strain-softening behavior was observed in all tests.

(6) The axial strength increased by 28–41% for the specimens confined by cast-in situ C-FRCM with overlapped or lap-spliced carbon fabrics while the strain at the peak load increased by 6–32%. When the specimens were confined by prefabricated C-FRCM, the axial strength increased by about 10% while the strain at the peak load increased by about 45%. Maximum load increased significantly due to enlarged cross-section.

Finally, the test setup used for tensile test in this study allows a rotational degree of freedom at each end while the fibers are free to slip inside the mortar similar to a clevis grip. Test results indicate that the current test setup properly allows the fibers to slip from the mortar without inducing any significant bending moment.

Acknowledgements
Not applicable.

Authors' contributions
DC: Overall research plan and control. SV: Leader of experimental program (column confinement tests). MO and UN: specimen fabrication and testing. SH: leader of experimental program (tensile tests). YK: fabrication method of meshes for precast specimens. All authors read and approved the final manuscript.

Authors' information
Donguk Choi, Professor, Department of Architectural Engineering, Hankyong National University, Anseong 17579, Republic of Korea.
Sorrasak Vachirapanyakun, Ph. D candidate, Department of civil and environmental system engineering, Konkuk University, Seoul 05029, Republic of Korea.
Munckhtuvshin Ochirbud, Graduated student, Department of Architectural Engineering, Hankyong National University, Anseong 17579, Republic of Korea.
Undram Naidangjav, Graduated student, Department of Architectural Engineering, Hankyong National University, Anseong 17579, Republic of Korea.
Sangsu Ha, Professor, Department of Architectural Engineering, Kangnam University, Yongin-si 446-702, Republic of Korea.
Youngho Kim, Professor, School of Food Biotechnology & Chemical Engineering, Hankyong National University, Anseong 17579, Republic of Korea.

Funding
Not applicable.

Availability of data and materials
Not applicable.

Declarations

Competing interests
The authors declare that they have no competing interests.

Author details
[1]Department of Architectural Engineering, Hankyong National University, Anseong 17579, Republic of Korea. [2]Department of Civil and Environmental System Engineering, Konkuk University, Seoul 05029, Republic of Korea. [3]Department of Architectural Engineering, Kangnam University, Yongin-si 446-702, Republic of Korea. [4]School of Food Biotechnology & Chemical Engineering, Hankyong National University, Anseong 17579, Republic of Korea.

Received: 8 April 2021 Accepted: 15 October 2021
Published online: 17 November 2021

References

AC434 (2013) Masonry and Concrete Strengthening Using Fabric-reinforced Cementitious Matrix (FRCM) and Steel Reinforced Grout (SRG) Composite Systems, ICC-ES.

ACI 549.4R (2013) Guide to design and construction of externally-bonded fabric-reinforced cementitious matrix (FRCM) systems for repair and strengthening concrete and masonry structures, American Concrete Institute, Farmington Hills, MI.

Al-Gemeel, A. N., & Zhuge, Y. (2018). Experimental investigation of textile reinforced engineered cementitious composite (ECC) for square concrete column confinement. *Construction and Building Materials, 174*, 594–602.

Arboleda, D., Carozzi, F. G., Nanni, A., & Poggi, C. (2016). Testing procedures for the uniaxial tensile characterization of fabric-reinforced cementitious matrix composites. *ASCE Journal of Composite Construction, 20*(3), 04015063.

ASTM D642. (2013). Standard Test Method for Density, Absorption, and Voids in Hardened concrete. ASTM International, West Conshohocken, PA.

Bellini, A., Shahreza, S. K., & Mazzotti, C. (2019). Cyclic bond behavior of FRCM composites applied on masonry substrate. *Composites, Part b: Engineering, 169*, 189–199.

Caggegi, C., Lanoye, E., Djama, K., Bassil, A., & Gabor, A. (2017). Tensile behaviour of a basalt TRM strengthening system: Influence of mortar and reinforcing textile ratios. *Composites, Part b: Engineering, 130*, 90–102.

Carozzi, F. G., Bellini, A., D'Antonio, T., de Felice, G., Focacci, F., Hojdys, L., Laghi, L., Lanoye, E., Micelli, F., Panizza, M., & Poggi, C. (2017). Experimental investigation of tensile and bond properties of Carbon-FRCM composites for strengthening masonry elements. *Composites, Part b: Engineering, 128*, 100–119.

D'Ambrisi, A., Feo, L., & Focacci, F. (2013). Experimental analysis on bond between PBO-FRCM strengthening materials and concrete. *Composites Part B., 44*, 524–532.

D'Antino, T., & Papanicolaou, C. (2018). Comparison between different tensile test set-ups for the mechanical characterization of inorganic-matrix composites. *Construction and Building Materials, 171*, 140–151.

Donnini, J., Chiappini, G., Lancioni, G., & Corinaldesi, V. (2019a). Tensile behavior of glass FRCM systems with fabric's overlap: Experimental results and numerical modeling. *Composite Structures, 212*, 398–411.

Donnini, J., Spagnuolo, S., & Corinaldesi, V. (2019b). A comparison between the use of FRP, FRCM and HPM for concrete confinement. *Composites, Part b: Engineering, 160*, 586–594.

Gong, T., Ahmed, A. H., Curosu, L., & Mechtcherine, V. (2020). Tensile behavior of hybrid fiber reinforced composites made of strain-hardening cement-based composites. *Construction and Building Materials, 262*, 120913.

Gonzalez-Libreros, J., Zanini, M. A., Faleschini, F., & Pellegrino, C. (2019). Confinement of low-strength concrete with fiber reinforced cementitious matrix (FRCM) composites. *Composites Part B, 177*, 107407.

Hadad, H. A., Erickson, B., & Nanni, A. (2020). Flexural analysis and design of FRCM-strengthened RC beams. *Construction and Building Materials, 244*, 118371.

Hadad, H. A., Nanni, A., Ebead, U. A., & Ek, R. A. (2018). Static and Fatigue Performance of FRCM-Strengthened Concrete Beams. *ASCE Journal of Composites in Construction, 22*(5), 04018033.
ISO 10406–2. (2015). *Fibre-reinforced polymer (FRP) reinforcement of concrete—est methods—Part 2: FRP sheets*. Switzerland.
Koutas, L. N., Tetta, Z., Bournas, D. A., & Triantafillou, T. C. (2019). Strengthening of concrete structures with textile reinforcing mortars: state-of-the-art review. *ASCE Journal of Composite Construction, 23*(1), 03118001.
KS L 5105. (2007). Testing method for compressive strength of hydraulic cement mortar, Korean Agency for Technology and Standards.
Larbi, A. S., Agbossou, A., & Hamelin, P. (2013). Experimental investigation about textile-reinforced concrete and hybrid solutions for repairing and/or strengthening reinforced concrete beams. *Composite Structures, 99*, 152–162.
Leone, M., Aiello, M. A., Balsamo, A., Carozzi, F. G., Ceroni, F., Corradi, M., Gams, M., Garbin, E., Gattesco, N., Krajewski, P., Mazzotti, C., Oliviera, D., Papanicolaou, C., Ranocchiai, G., Roscini, F., & Gaenger, D. (2017). Glass fabric reinforced cementitious matrix: Tensile properties and bond performance on masonry substrate. *Composites, Part b: Engineering, 127*, 16–214.
Mander, J., Priestley, J., & Park, R. (1988). Theoretical stress-strain model for confined concrete. *Journal of Structural Engineering, 114*(8), 1804–1826.
Mazzuca, S., Hadad, H. A., Ombres, L., & Nanni, A. (2019). Mechanical characterization of steel-reinforced grout for strengthening of existing masonry and concrete structures. *ASCE Journal of Materials, 31*(5), 0019037.
Nadianjav U., Sangsu Ha, Orchirbud M., Choi D. (2021) Mechanical characterization of PBO fabric reinforced cementitious matrix, Journal of Korea Concrete Institute, *in press* (in Korean).
Orchirbud, M., Choi, D., Nadianjav, U., Ha, S.-S., & Lee, C.-Y. (2020). Mechanical characterization of a FRCM system with aramid fiber fabric embedded in green high-strength cementitious matrix. *Journal of Asian Concrete Federation, 6*(2), 1–13.
Peled, A., Mobasher, B., & Cohen, Z. (2009). Mechanical properties of hybrid fabrics in pultruded cement composites. *Cement & Concrete Composites, 31*, 647–657.
Raoof, S. M., Koutas, L. N., & Bournas, D. A. (2016). Bond between textile-reinforced mortar (TRM) and concrete substrates: Experimental investigation. *Composites: Part B, 98*, 350–361.
Rilem TC 232-TDT. (2016). Test methods and design of textile reinforced concrete. *Materials and Structures, 49*, 4923–4927.
Santis, S. D., Ceroni, F., de Felice, G., Fagone, M., Ghiassi, B., Kwiecien, A., Lignola, G. P., Morganti, M., Santandrea, M., Valluzzi, M. R., & Viskovic, A. (2017). Round Robin test on tensile and bond behavior of Steel Reinforced Grout systems. *Composites, Part b: Engineering, 127*, 100–120.
Tello, N., Alhoubi, Y., Abed, F., El-Refai, A., & El-Maaddawy, T. (2021). Circular and square columns strengthened with FRCM under concentric load. *Composite Structures, 255*, 113000.
You, Y.-J., et al. (2020). Strengthening of concrete element with precast textile reinforced concrete panel and grouting material. *Materials, 13*(17), 13173856.
Younis, A., & Ebead, U. (2018). Bond characteristics of different FRCM systems. *Construction and Building Materials, 175*, 610–620.

Publisher's Note